

Biochar-Assisted Iron-Mediated Water Electrolysis Process for Hydrogen Production

Gidon Amikam, Noga Fridman-Bishop, and Youri Gendel*

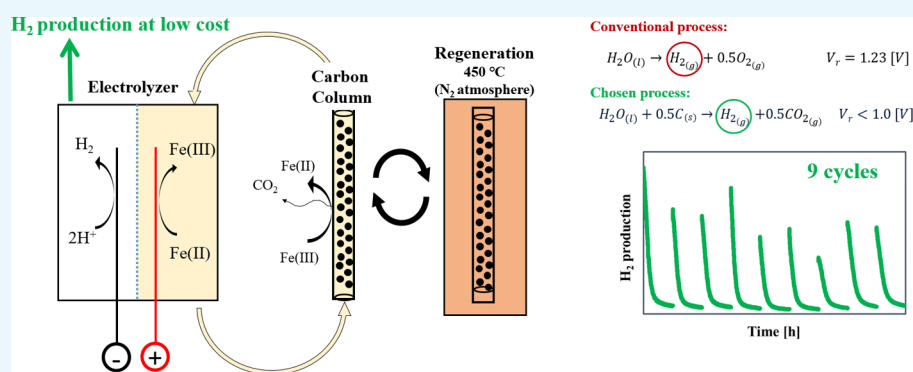
Cite This: *ACS Omega* 2020, 5, 31908–31917

Read Online

ACCESS |

Metrics & More

Article Recommendations



ABSTRACT: The biochar-assisted water electrolysis process for hydrogen gas production is reported. The H₂ generation is performed in a divided electrolysis cell in which the hydrogen evolution reaction occurs on a cathode and ferrous iron oxidation on an anode. Electrochemically produced Fe(III) species are reduced back to ferrous form in a reaction with biochar concentrated in a packed-bed column through which an acidic anolyte (FeCl₃) solution is continuously recirculated. During the operation of the proposed process with commercial charcoal, the oxidation of carbon resulted in an accumulation of oxygen-containing groups on the carbon surface that leads to charcoal deactivation. Thermal treatment of the charcoal at 250, 350, and 450 °C in a nitrogen atmosphere resulted in reactivation of carbon, and the best results (≈80% reactivation) were achieved after 3 h of treatment at 450 °C. Nine successful cycles of electrolysis-charcoal regeneration were performed in this study. A ≈98% current efficiency for hydrogen production was achieved at a current density of 50 mA/cm². Much higher current densities can be obtained using the proposed technique as the anodic process of ferrous iron oxidation is decoupled from the carbon oxidation process. The CO₂ production rate achieved in this study was up to 98% of a stoichiometric value proposed for the iron-mediated carbon-assisted water electrolysis process.

1. INTRODUCTION

Hydrogen gas is a “clean” fuel because the major product of its reaction with oxygen in internal combustion engines and fuel cells is water. Hydrogen gas is also highly attractive for the conversion and storage of renewable energy due to its high gravimetric energy density. The higher heating value (HHV) of hydrogen is about 39.405 Wh/kg, which is higher than the HHVs of gasoline and methane (13.19 and 15.42 Wh/kg, respectively).^{1,2} The annual production of hydrogen is ≈65 million metric tons, and its consumption increases by 6% annually.^{1–3} Today, over 90% of hydrogen gas is produced from fossil fuels by natural gas reforming and coal gasification processes. The largest consumers of H₂ are artificial fertilizer and petroleum industries (47 and 37%, respectively).^{1,3} The H₂ gas is also used in metal production, methanol production, food processing, and electronics.

The substantial drawback in hydrogen production from fossil fuels is the co-current production of CO₂ and its

accumulation in the atmosphere. Another disadvantage is the low purity of produced hydrogen gas. For example, in steam reforming of natural gas, 7.05 kg of CO₂ is produced per kilogram of hydrogen.³

High-quality hydrogen can be produced by electrochemical conversion of water into hydrogen and oxygen via the water electrolysis (WE) process.^{1,4,5} An important advantage of WE technologies is that they can be integrated into renewable energy production and storage processes. Unfortunately, today only ≈4% of the overall hydrogen is produced using the WE

Received: October 1, 2020

Accepted: November 26, 2020

Published: December 7, 2020



techniques due to their intensive energy consumption.^{1,4,5} The cost of distributed electrolytic hydrogen was 3.90 USD/kg H₂ in 2015, and the targeted 2020 cost is 2.3 USD/kg H₂.⁶ The state-of-the-art energy consumption for electrochemical hydrogen production is 57–60 kWh/kg H₂, and the targeted values for years 2020 and 2023 are 52 and 50 kWh/kg H₂, respectively.⁷ The energy requirement of water electrolysis (enthalpy change, ΔH) comprises the electric energy (ΔG , that corresponds to the Gibbs' free energy change) and thermal energy (Q , the product of the process temperature (T) and the entropy change (ΔS)) (eq 1)

$$\Delta G = \Delta H - Q = \Delta H - T \cdot \Delta S \quad (1)$$

Figure 1 shows the variation of ΔH , $T \cdot \Delta S$, and ΔG with temperature. The total energy demand for the process (ΔH) is

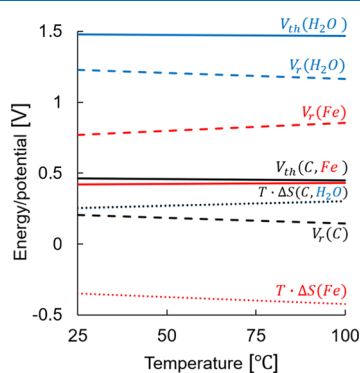


Figure 1. Reversible potential (V_r), thermoneutral potential (V_{th}), and heat energy ($T \cdot \Delta S$) at varied temperatures of (i) water electrolysis; (ii) carbon-assisted water electrolysis; and (iii) carbon-assisted iron-mediated water electrolysis.

almost independent of temperature. However, the values of $T \cdot \Delta S$ and ΔG increase and decrease at higher temperatures, respectively.^{1,8} At standard temperature (298.15 K) and pressure (1 atm), the values of ΔG , ΔS , and ΔH for water electrolysis are 237.21 kJ/mol, 0.1631 kJ/(mol.K), and 285.84 kJ/mol, respectively.⁸ The lowest cell potential required for the WE is known as the reversible potential (V_r) (eq 2)

$$V_r = \frac{\Delta G}{z \cdot F} \quad (2)$$

where z is the number of electrons transferred per mole of H₂ ($z = 2$ for WE) and F is the Faraday constant (96 485 C/mol e⁻).

The thermoneutral voltage (V_{th}) is defined as the minimum voltage required for WE to occur at adiabatic conditions, where all of the reaction enthalpy is provided by electricity.^{1,8}

$$V_{th} = V_{\Delta H} = \frac{\Delta H}{z \cdot F} \quad (3)$$

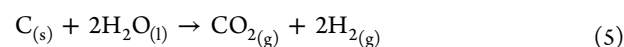
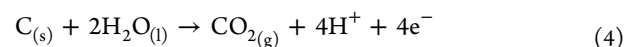
At standard conditions, the V_r and V_{th} values for WE are 1.229 and 1.481 V, respectively.^{1,8} When the electrolysis cell is operated between V_r and V_{th} , the process is endothermic. When the cell potential is greater than V_{th} , the process is exothermic.^{1,8}

1.1. Chemical-Assisted Water Electrolysis. The goal of the chemical-assisted water electrolysis processes is to decrease the energy consumption of the “conventional” WE process. One of the promising ways to decrease energy requirements of water electrolysis is to replace the oxygen evolution reaction

with less energy demanding anodic processes. Electrochemical oxidation of aqueous sulfur dioxide (SO₂) is an electrolytic process where sulfur dioxide is oxidized to sulfuric acid on the anode instead of water oxidation.^{9,10} The V_r of the SO₂-assisted water electrolysis process is lower than in the un-assisted WE process (0.158 V vs 1.23 V, respectively). Currently, the process is still under development and suffers from several limitations and drawbacks: (1) a lack of fundamental understanding of the mechanism behind the electrochemical oxidation of sulfur dioxide; (2) crossover of the electrolyte (SO₂) through the cell membrane; (3) high costs and instability of reactor materials and catalysts; and (4) relatively low current densities (≈ 200 mA/cm²).¹⁰

In the liquid-hydrocarbon-assisted water electrolysis process, the hydrocarbon solution is recirculated through the anodic compartment of the electrolysis cell where it is oxidized on the anode to carbon dioxide (CO₂).¹ A variety of alcohols and liquid hydrocarbons (e.g., methanol, ethanol/bioalcohol, formic acid, glycerol, ethylene glycol, and biomass/high-molecular-weight hydrocarbon) can be used as energy sources in electrolysis processes for hydrogen production.¹ Every type of hydrocarbon has a different V_r value. For example, the V_r values of methanol, glycerol, and ethanol are 0.02, 0.08, and 0.24 V, respectively.¹ Although relatively high current densities at relatively low potentials have been reported in the literature (0.2–1 A/cm² at 0.8–1.2 V), the process still has some serious drawbacks, such as the availability and cost of alcohol and organic solutions, high costs and instability of cell materials and catalysts, degradation of membranes, incomplete conversion of hydrocarbons to CO₂, and evolution of toxic byproducts.¹

1.2. Carbon-Assisted Water Electrolysis (CAWE). First investigations of CAWE were done in 1932 by C.S. Lynch and A.R. Collett who performed electrolytic oxidation of Pittsburg coal in 3 N NaOH solution with copper, nickel, lead and platinum electrodes.^{11,12} Later, many studies on coal electrolysis in alkaline and acidic media were performed to study the performance of the process at different temperatures and with different catalysts and carbon types (e.g., coal, graphite, anthracite, and peat).^{12–16} In these studies, carbon dioxide and carbon monoxide were identified as the major products of coal oxidation on the Pt anode, and hydrogen was always a major cathodic product. Coughlin and Farooque^{13–16} postulated the half-cell reaction of carbon in coal-assisted water electrolysis (eq 4) and the overall reaction of this process (eq 5)



The reversible (V_r) and thermoneutral (V_{th}) potentials of CAWE are 0.21 and 0.421 V (vs standard hydrogen electrode (SHE)) respectively, which are significantly lower than the corresponding potentials of water electrolysis (i.e., 1.23 and 0.148 V vs SHE, respectively).^{16,17} For this reason, the energy demand of CAWE is expected to be significantly lower than that of other WE technologies.^{11,13–19}

The exact mechanisms of CAWE are unknown. Dhooge et al.²⁰ observed that ferric ions act as a catalyst in CAWE. In accordance with the mechanism proposed by Dhooge et al.,²⁰ the coal is oxidized by ferric ions, producing ferrous ions and carbon dioxide (eq 6). The ferrous ions, in turn, are oxidized

back to the ferric form by anodic oxidation as described by eq 7.²⁰

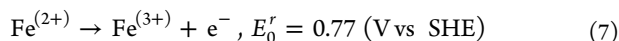
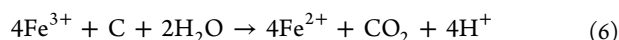


Figure 1 shows the V_r and V_{th} for (i) water electrolysis, (ii) carbon-assisted water electrolysis, and (iii) iron-mediated water electrolysis at varied temperatures. The values were calculated using eqs 1–3 and 8–14.

To calculate the values of enthalpy of reactions at varied temperatures, eq 8 was used.²¹

$$dH = C_p dT \quad (8)$$

where C_p is the heat capacity of the reactant or product at constant pressure. The dependency of C_p on temperature is described by eq 9.²¹

$$C_p = a + bT + \frac{c}{T^2} \quad (9)$$

where a , b , and c coefficients have specific values for oxygen, CO_2 , and hydrogen gases, and their values can be found in Atkins et al.²¹

Integration of eq 8 between the initial and the final temperature results in eq 10

$$H_{(T_f)} = H_{(T_i)} + a(T_f - T_i) + \frac{1}{2}b(T_f^2 - T_i^2) - c\left(\frac{1}{T_f} - \frac{1}{T_i}\right) \quad (10)$$

To calculate the entropy values at varied temperatures, eq 11 was used.

$$dS = \frac{C_p}{T} dT \quad (11)$$

Integration of eq 11 between the initial and the final temperature results in eq 12

$$S_{(T_f)} = S_{(T_i)} + a \times \ln\left(\frac{T_f}{T_i}\right) + b(T_f - T_i) - \frac{c}{2}\left(\frac{1}{T_f} - \frac{1}{T_i}\right) \quad (12)$$

Since the ΔS and ΔH are the state functions, it is possible to calculate the ΔH and ΔS for reactions of interest using eqs 13 and 14

$$\Delta H_{R(T_f)} = \Delta H_{\text{cooling(reactants)}}(T_f \text{ to } T_i) + \Delta H_R(T_i) + \Delta H_{\text{heating(products)}}(T_i \text{ to } T_f) \quad (13)$$

$$\Delta S_{R(T_f)} = \Delta S_{\text{cooling(reactants)}}(T_f \text{ to } T_i) + \Delta S_R(T_i) + \Delta S_{\text{heating(products)}}(T_i \text{ to } T_f) \quad (14)$$

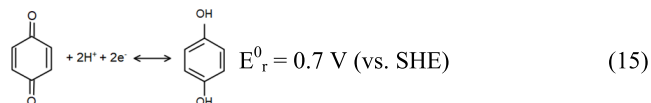
It was assumed in calculations of V_r and V_{th} for the iron-assisted water electrolysis that the heat capacity of iron species is negligible.

According to Figure 1, the iron-mediated CAWE, with the thermodynamic minimum potential for operation of $V_r = 0.77$ V, can be 50% more energy efficient than the conventional water electrolysis for which the thermodynamic minimum potential for adiabatic operation is $V_{th} = 1.481$ V.

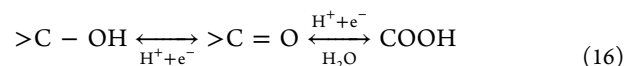
Within the last 2 decades, there has been a renewal of the intensive research in the field of CAWE, as indicated by the

exponentially increasing number of relevant scientific publications. The latest studies in CAWE focused mainly on the development of catalysts, redox mediators, cell architectures,^{1,21–25} and investigation of the process at varied operational conditions²⁶ (e.g., types of carbon, applied potentials, and electrolyte compositions).^{1,22,27–31} In spite of the intensive research on CAWE, the process still suffers from many drawbacks and limitations, and the most challenging are (1) the low current densities and (2) the deactivation of carbon with the electrolysis duration.^{1,32}

The exact reason for the gradual decline of current density observed in CAWE for all types of investigated carbons is still unknown, but it was associated with two main phenomena: (1) depletion of reactive impurities (like FeS_2) and (2) changes in the morphology and chemical structure of the carbon surface.¹³ The first phenomenon is less likely since it is inconsistent with the results of long-term (~ 450 h) experiments performed by Coughlin and Farooque.¹⁶ The second phenomenon in CAWE is more complex and still unclear. The carbon surface may contain many different types of acidic oxygen groups (e.g., carboxylic acids, lactones, lactols, phenol, anhydrides), basic oxygen groups (e.g., quinone, chromene, pyrone), and neutral oxygen groups (like carbonyl and ether).³³ In addition to oxygen-containing functional groups, nitrogen- (e.g., pyridine, pyrrole, pyridine) and sulfur-containing groups (e.g., thioquinone, sulfoxide, thiolactone, thiophenol) are often present on the carbon surface.^{33,34} Some functional surface groups of carbons are electrochemically active, and these groups are especially important in electrochemical processes. The most known electrochemically active surface group in carbons is a quinone–hydroquinone couple (eq 15)³⁴



Fan et al.³⁵ showed that in anodic oxidation of carbons hydroxyl groups could be reversibly oxidized into ketone groups and further into carboxylic groups (eq 16)



Coughlin et al.¹⁶ reported on the increasing percentage of oxygen in the chemical composition of coal during the coal-assisted water electrolysis. In addition, the authors noted that treatment of the reacted coal with acetone could restore to some extent its electrochemical activity and decrease the weight percentage of oxygen in the coal.¹⁸ Unfortunately, the mechanism of acetone treatment in carbon reactivation was not explained in this study.

1.3. Biochar for Carbon-Assisted Water Electrolysis. Charcoal (the most common example of biochar) has been produced from wood for centuries, but only recently has it been realized as a highly promising strategy for carbon mitigation from the earth's atmosphere via the actual removal of CO_2 gas.^{36–39} The concept includes the pyrolysis (or hydrothermal carbonization) of biomass for biochar production and its application to agricultural or forest soils. The estimated half-life of pyrolytic char in the soil is from 100 to more than 1000 years.³⁹ If the safety of biochar application to soils as well as the effectiveness of the biochar approach on the global CO_2 mitigation was proven, one would expect the

worldwide development of the technology in the next decades. Consequently, it is envisaged in this strategy that biochar will become cheap and available material to produce many chemicals, including hydrogen gas for energy storage operations and as a raw chemical for many industries. Part of the biochar can be utilized in CO₂-neutral carbon-assisted water electrolysis for hydrogen production prior to its application to soil. Production of charcoals is also a sustainable solution for the utilization of organic fractions of agricultural and municipal solid wastes (and slurries from wastewater treatment plants).

In 2019, Chen et al.⁴⁰ proposed the utilization of biochar for carbon-assisted water electrolysis. In this study, powdered biochar was electrolyzed in a divided electrolysis cell using H₂SO₄ and H₂SO₄/NaCl electrolytes. The reactivation of carbon was done using heat treatment at 850 °C and via the CO₂ gasification.⁴⁰

The present study was dedicated to the proof of concept and investigation of the process for low-cost electrochemical production of hydrogen gas using a biochar-assisted iron-mediated water electrolysis process.

1.4. Proposed Process. Figure 2 represents the proposed electrochemical process that comprises three major units: (1)

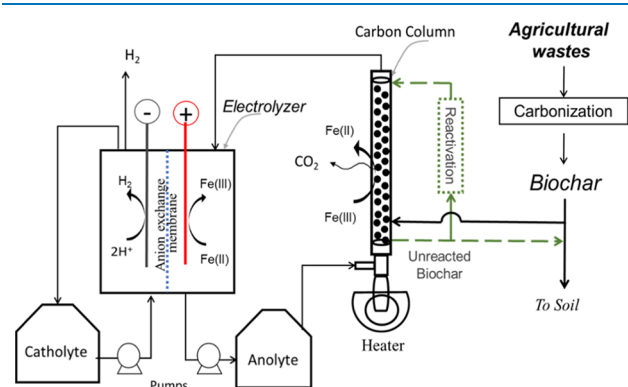


Figure 2. Proposed process for iron-mediated biochar-assisted water electrolysis for hydrogen production.

hydrothermal or pyrolytic biochar production from agricultural wastes (not in the scope of this study); (2) a packed-bed column filled with the produced biochar; and (3) a divided electrolysis cell for hydrogen production.

Hydrogen gas is produced on the cathode in the divided electrolysis cell shown in Figure 2. A cation or an anion exchange membrane is required to prevent reduction of Fe(III) iron to Fe(II) form (and even elemental iron formation^{41,42}) on the cathode that would result in a loss of current efficiency for the hydrogen evolution reaction. An acidic aqueous solution (e.g., hydrochloric acid) is recirculated through the cathodic compartment of the cell. The anolyte comprises an aqueous acidic solution of ferrous ions, which are oxidized to ferric ions on the anode. Ferric ions are reduced back into the ferrous form via the reaction with biochar granules packed in a separate column, as shown in Figure 2. Residual biochar (unreacted in the electrochemical system) is either reactivated using the thermal treatment in an inert atmosphere or applied into the agricultural soils to improve crop productivity and for CO₂ sequestration from the atmosphere. The energy for thermal reactivation can be obtained from partial combustion of biochar or using other sources of heat (if available).

2. RESULTS AND DISCUSSION

2.1. Batch-Mode Experiments of Fe(III) Reduction by Charcoal.

Figure 3 and Table 1 show the results of the Fe(III)

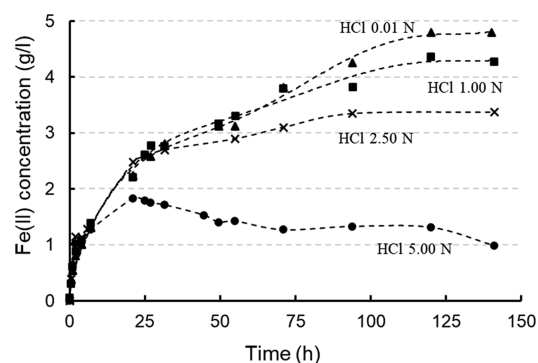


Figure 3. Fe(III) reduction by 150 g/L biochar at varied HCl concentrations. [FeCl₃]₀ = 20 g/kg H₂O, volume = 100 mL, temperature = 25 °C, shaking speed = 125 rpm.

Table 1. Ferrous Ion Production in the Presence of 150 g/L of Charcoal at Varied Electrolyte Compositions^a

| electrolyte composition | Fe(II) concentration after 21 h (g/L) |
|---------------------------------------|---------------------------------------|
| HCl 5 N | 1.823 |
| HCl 2.5 N | 2.475 |
| HCl 1 N | 2.207 |
| HCl 0.1 N | 2.302 |
| HCl 0.01 N | 2.234 |
| HCl 0.01 N, NaCl 1 M | 2.515 |
| H ₂ SO ₄ 0.01 N | 0.416 |
| H ₂ SO ₄ 1 N | 0.388 |

^aInitial ferric ions concentration = 20 g/kg H₂O, slurry volume = 100 mL, temperature = 25 °C.

reduction experiments performed at varied concentrations of HCl and H₂SO₄ acids in FeCl₃ and Fe₂(SO₄)₃ solutions ([Fe(III)]₀ = 20 g Fe/L), respectively. The reaction of charcoal with ferric ions in hydrochloric acid was much faster than in sulfuric acid. In fact, no difference was observed in experiments conducted at H₂SO₄ concentrations of 0.01 and 1.0 N, and in both experiments, only ≈2% of ferric iron was reduced into the ferrous form after 21 h. In contrast, more than 10% of Fe(III) was reduced in HCl solutions. No significant difference was observed in Fe(III) reduction rates in experiments conducted with HCl concentrations in the range of 0.01–2.5 N. The faster reaction of carbon with ferric species in HCl acid than in a H₂SO₄ solution can be attributed to different complexation of Fe²⁺ and Fe³⁺ ions by Cl⁻ and SO₄²⁻ species. However, the exact reason is unknown and requires detailed investigation.

In all experiments shown in Figure 3, the concentration of ferrous iron reached the maximum, which indicates carbon deactivation. Higher concentrations of HCl resulted in lower final concentrations of ferrous iron. This can be explained by the fact that carbon oxidation results in generation of protons (eqs 4 and 6) and higher acidity leads to inhibition of the process. The decrease in Fe²⁺ concentration obtained in the experiment conducted with 5 N of HCl is probably due to the precipitation of iron chloride species.

The reduction rate observed at 5 N of HCl was significantly lower than at other HCl concentrations. Consequently, it was

decided to operate the continuous CAWE system with the HCl concentration of 1 M.

2.2. Preparation of Deactivated Biochar. Figure 4 shows the results of the two-stage operation of a larger biochar

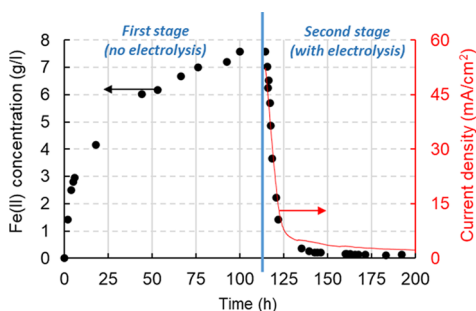


Figure 4. Experimental results of the biochar-assisted iron-mediated electrolysis process.

column in the process shown in Figures 2 and 8 (see Section 4). During the first stage of the process, the system succeeded to convert around 40% of ferric ions into the ferrous iron form. Relatively high current densities ($\sim 52 \text{ mA/cm}^2$) were observed at the beginning of the electrochemical stage (Figure 4), but after 20 h of operation, the current density decreased to $\approx 5.0 \text{ mA/cm}^2$ due to gradual biochar deactivation.

The current density obtained in this study is significantly higher than the current density of $12.3\text{--}7.3 \text{ mA/cm}^2$ reported by Chen et al.⁴⁰ for continuous biochar-assisted WE conducted at a cell potential of 1.0 V (20 g/L of $37\text{--}74 \mu\text{m}$ biochar particles, $[\text{NaCl}] = 0.25 \text{ M}$). The difference is due to the iron mediation of the process applied in this study and because significantly higher volumetric loadings of carbon can be obtained in the system with a packed-bed column compared to suspension electrodes. The kinetics of biochar oxidation by iron strongly depends on the size of biochar particles. Operation of the proposed process with smaller biochar granules is expected to result in significantly higher current densities of the hydrogen production reaction. During overall 85 h of electrolysis, the charge that passed in the electrolysis cell was 38.7 (kC), which is equivalent to $\approx 4.4 \text{ L}$ of hydrogen gas at $25 \text{ }^\circ\text{C}$, assuming an ideal gas and 90% current efficiency (see Table 2). Table 2 lists the values of current efficiency for

Table 2. Current Efficiency for the Hydrogen Evolution Reaction Obtained in CAWE Experiments Conducted in the System Shown in Figure 8

| current density (mA/cm^2) | current efficiency for H_2 production (%) |
|--------------------------------------|--|
| 12.5 | 77.4 |
| 25 | 89.8 |
| 37.5 | 97.3 |
| 50 | 97.8 |

H_2 production measured using a water displacement method at varied applied current densities. Current efficiency as high as $\approx 98\%$ was achieved at a current density of 50 mA/cm^2 . A lower current efficiency was obtained for lower current densities due to the crossover of ferrous iron ions from the anolyte into the catholyte compartment and a consequent parasitic Fe(III) reduction on the cathode. This unwanted process can be minimized if the electrolysis cell is divided by an anion exchanging membrane.

2.3. Thermal Reactivation of Biochar. Figure 5A shows the results of Fe(III) reduction experiments conducted on biochar regenerated for 6 h at 250 , 350 , and $450 \text{ }^\circ\text{C}$ in the nitrogen atmosphere.

As it is shown in Figure 5, a higher regeneration temperature resulted in better regeneration efficiency and the biochar sample regenerated at $450 \text{ }^\circ\text{C}$ outperformed the original (as received) biochar. The regeneration at temperatures higher than $450 \text{ }^\circ\text{C}$ might result in faster and better regeneration of carbons than at $450 \text{ }^\circ\text{C}$. On the other hand, the energy demand of the thermal treatment is higher at higher temperatures. Consequently, it was decided in this study to perform biochar regeneration at $450 \text{ }^\circ\text{C}$.

Figure 5B shows biochar temperature and accumulation of CO_2 inside the NaOH solution vs the biochar regeneration time obtained at $450 \text{ }^\circ\text{C}$. According to Figure 5B, the most intensive production of CO_2 occurred once the biochar temperature reached $450 \text{ }^\circ\text{C}$. During the first 3 h of thermal treatment at $450 \text{ }^\circ\text{C}$, almost 90% of overall CO_2 generated within 7.5 h was released from the biochar. Consequently, it was decided to perform 4 h long regeneration steps in electrolysis-regeneration experiments.

Tables 3 and 4 and Figure 6 show the results of X-ray photoelectron spectroscopy (XPS) analysis conducted on (i) as-received biochar, (ii) biochar deactivated in biochar-assisted iron-mediated water electrolysis, and (iii) biochar regenerated at $450 \text{ }^\circ\text{C}$.

According to Figure 6, and Tables 3, and 4, the oxidation of biochar by ferric chloride in the electrochemical stage of the proposed process resulted in the accumulation of oxygen atoms on the carbon surface. The amount of C–O bonds increased from 15.60 to 24.48% (Table 3) and the amount of oxygen from 15.3 to 24.7% (Table 4). This is apparently the major reason for carbon deactivation because these groups prevent the reaction of carbon with ferric iron ions. The same conclusion follows from Table 5 that details the chemical composition of charcoal before and after the deactivation. Results concentrated in Table 5 have been obtained by the elemental analysis method using the Flash 2000 organic elemental analyzer (Thermo Scientific).

Oxygen-containing groups can be desorbed from carbon surfaces using heat treatment in inert atmospheric conditions.³⁴ Therefore, the thermal treatment removes the oxygen groups from the used biochar surface as can be seen in Tables 3–5. This way, the thermal treatment regenerates the biochar in the proposed process. Similar surface chemistry processes were observed previously by Chen et al.⁴⁰ in the carbon-assisted water electrolysis process performed without an iron mediator in $\text{H}_2\text{SO}_4/\text{NaCl}$ solutions using a divided electrochemical cell operated with a powdered biochar-made slurry anode.

2.4. Cycling CAWE-Regeneration Operations. Figure 7 and Table 6 show the results of nine cycles of electrolysis-charcoal regeneration operations performed using the system shown in Figure 8 (see Section 4). As it is shown in Figure 7, the proposed CAWE process was successfully performed for nine cycles and a maximal current density of $\approx 8\text{--}20 \text{ mA/cm}^2$ was achieved at different cycles. It should be noted that maximum current density was significantly higher ($\approx 52 \text{ mA/cm}^2$) in experiments that were conducted with the bigger charcoal column. This is because the current and energy density of the proposed process are in direct relation to the

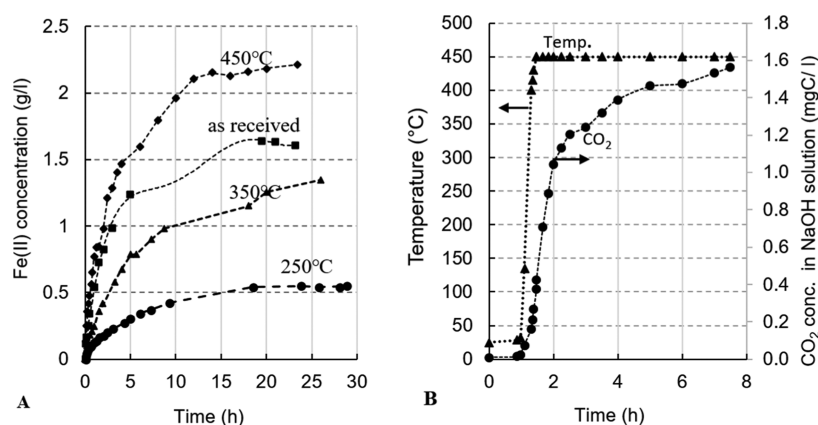


Figure 5. Results of batch experiments for ferrous iron production via Fe(III) reduction by the biochar regenerated at varied temperatures (A), and variation of biochar temperature and accumulation of CO₂ inside the NaOH solution vs time in biochar regeneration at 450 °C (B).

Table 3. Surface Chemistry of Original, Deactivated, and Regenerated Charcoal Obtained by the XPS Analysis

| parameter/biochar | surface groups/bonds | | | | | | |
|-------------------------|----------------------|---------|-------|-------|----------|--------|-------------|
| | C=C | C-C/C-H | C-O | C=O | C-O-C*=O | OH-C=O | -O-C-O-II O |
| binding energy (eV) | 283.95 | 285.0 | 286.2 | 287.2 | 288.36 | 289.39 | 240.49 |
| as-received biochar (%) | | 64.4 | 15.3 | 9.1 | 5.2 | 4.1 | 1.9 |
| deactivated biochar (%) | 19.2 | 45.5 | 24.7 | 5.3 | 2.8 | 1.95 | 0.57 |
| regenerated biochar (%) | | 80.2 | 13.1 | 3.5 | 0.9 | 1.4 | 0.9 |

Table 4. Atomic Concentrations (in %) of C, O, N, and Cl Elements in Original, Deactivated, and Regenerated Charcoal Obtained by the XPS Analysis

| element | atomic concentration (%) | | |
|---------|--------------------------|---------------------|---------------------|
| | as-received biochar | deactivated biochar | regenerated biochar |
| C | 82.59 | 77.04 | 86.51 |
| O | 15.60 | 20.48 | 10.26 |
| N | 0.67 | 0.13 | 0.10 |
| Cl | 0.05 | 0.84 | 1.60 |

amount of charcoal in the system, i.e., the current density can be increased by increasing the mass of charcoal in a column.

The charcoal regeneration efficiency decreased significantly after the first cycle as becomes evident from the accumulation rates of Fe(II) iron obtained within the first stage of the process (Figure 7A) and the current density obtained within the electrochemical operations (Figure 7B). However, the regeneration efficiency was always higher than 45% as appears from the calculation of charge that was conducted in each electrochemical cycle within 15 h of electrolysis (Table 6). In cycles 8 and 9, the regeneration efficiency was as high as ~80%. This is because the regeneration setup was slightly modified during cycles 8 and 9. To improve the regeneration efficiency, the inlet and outlet of the tubular furnace were sealed with the heat-retarding material.

Unfortunately, it was impossible to quantify the amount of biochar reacted within each cycle shown in Figure 7B. This is because the maximal theoretical loss of carbon in every electrolysis-regeneration step was less than 2% (assuming CO₂ is the only product of carbon oxidation). In addition, the biochar becomes filled with iron species and NaCl that increase the carbon weight. The final weight of the biochar in the column was 19.33 g, which corresponds to a weight reduction of 2.5 g. Consequently, the real biochar loss within 9 cycles was at least 64% of the theoretical value (3.9 g)

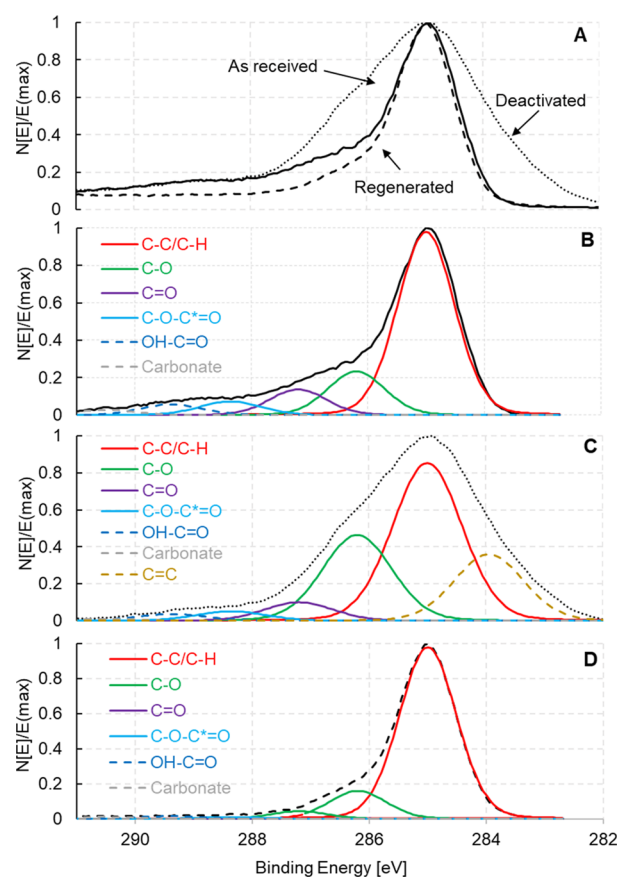


Figure 6. Results of (A) XPS spectra of the C 1s region for all types of biochar and XPS data as obtained for C 1s curve fitting for (B) original, (C) deactivated, and (D) regenerated charcoal.

calculated from eq 6 for the overall charge of 31 197 C (Table 6).

Table 5. Chemical Composition (wt %) and Ash Content Obtained from Elemental Analysis (Flash 2000 Organic Elemental Analyzer, Thermo Scientific) of Commercial Charcoal Produced from the Apple Tree Wood Before and After Deactivation in Iron-Mediated Electrochemical Oxidation

| charcoal/element | N (%) | C (%) | H (%) | S (%) | O (%) | ash content (%) |
|----------------------|-------|-------|-------|-------|-------|-----------------|
| as-received charcoal | 0.18 | 78.19 | 3.52 | 0.00 | 13.31 | 2.8 |
| deactivated charcoal | 0.05 | 57.93 | 2.86 | 0.00 | 39.4 | 0 |

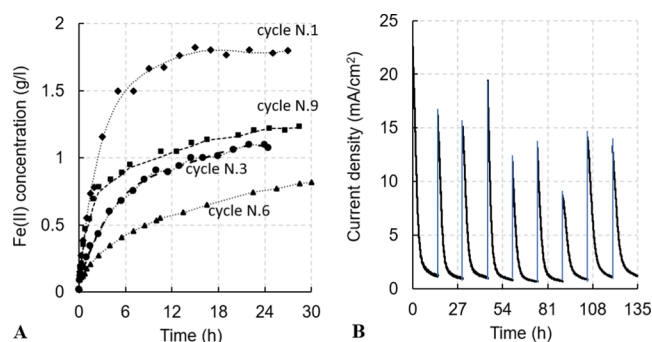


Figure 7. Concentration of ferrous iron (A) and current densities (B) obtained in nine electrolysis-regeneration operations of the biochar-assisted iron-mediated water electrolysis process.

From the stoichiometry of the CAWE process (eqs 4–7), and assuming that C^0 (carbon with the oxidation state of 0) and CO_2 are the only reactant and product (respectively) of the process, the charge/ CO_2 ratio (mol_e^-/mol_{CO_2} , Table 6) should equal 4. Interestingly, a value as high as 4.12 was obtained in the first cycle (Table 6). The reasons for this result might be experimental errors and the fact that C–H carbon (oxidation state –1) might be oxidized in the process. This hypothesis is supported by the results of elemental analysis of original and deactivated carbons (Table 5) and the XPS (Tables 3 and 4 and Figure 6), which show that the amount of hydrogen and C–C/C–H bonds on the carbon surface decreased during the electrolysis and increased within the regeneration steps.

In addition to CO_2 , many organic compounds were formed during the process. The results of the gas chromatography-flame ionization detector (GC-FID) analysis showed the presence of more than 5000 compounds in the NaOH solutions applied in the study. Table 7 concentrates the data for nine carboxylic acids that were determined in the CO_2 -absorbing solutions during the electrolysis and regeneration steps of cycle number 9 of electrolysis-regeneration operations. It is important to note that all organic acids listed in Table 7

Table 6. Electric Charge and Amounts of Carbon Dioxide Obtained during 15 h of Electrolysis in Nine Cycles of the Biochar-Assisted Iron-Mediated Water Electrolysis Process

| | cycle number | | | | | | | | |
|---|--------------|-------|------|------|-------|------|-------|-------|------|
| | 1 | 2 | 3 | 4 | 5 | 6 | 7 | 8 | 9 |
| charge passed during 15 h of electrolysis (C) | 4972 | 3574 | 3577 | 3307 | 2380 | 2644 | 2751 | 4064 | 3928 |
| CO_2 gas produced during each cycle (mmol) | 12.5 | 13.75 | 12.5 | 10 | 11.25 | 12.5 | 13.75 | 11.25 | 12.5 |
| charge- to- CO_2 ratio (mol_e^-/mol_{CO_2}) | 4.12 | 2.7 | 2.92 | 3.23 | 2.26 | 2.21 | 2.08 | 3.93 | 3.35 |

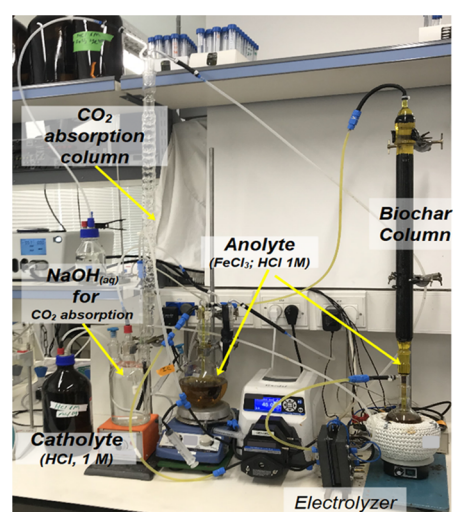


Figure 8. Experimental system for biochar-assisted iron-mediated water electrolysis.

Table 7. Carboxylic Acids That Were Produced during the Biochar-Assisted Iron-Mediated Water Electrolysis Process

| carboxylic acid | amount produced in cycle no. 9 (mg) |
|-----------------|-------------------------------------|
| acetic acid | 2.78 |
| propionic acid | 2.5 |
| isobutyric acid | 3.05 |
| butyric acid | 2.40 |
| isovaleric acid | 2.90 |
| valeric acid | 8.05 |
| isocaproic acid | 0.54 |
| hexanoic acid | 2.64 |
| heptanoic acid | 0.21 |

were determined in both CO_2 absorption units operated in series.

Consequently, some quantities of all acids were not trapped in the experiment and actual amounts of carboxylic acids produced during the process might exceed the values listed in Table 7. It is also important to note that the formation of organic compounds could be due to the chemical decomposition of biochar by an acidic NaCl solution in parallel to biochar oxidation by Fe(III) species.

3. CONCLUSIONS

The biochar-assisted iron-mediated electrolysis process with decoupled anodic oxidation of iron and its reduction in the packed-bed biochar column has been proposed and investigated in this study. The proposed process utilizes biochar produced from agricultural wastes in the carbon-assisted water electrolysis. Deactivation of biochar, previously reported in many studies, was shown to occur due to the accumulation of

oxygen-containing groups on the biochar surface. The reactivation of charcoal was successfully achieved (up to 80%) by the thermal treatment of charcoal in a nitrogen atmosphere at 450 °C. The energy for reactivation can be obtained from partial combustion of biochar or using other heat sources (if available). Current densities obtained in the proposed process depend on the amount of biochar in the system. In this study, $\approx 98\%$ current efficiency for hydrogen production was achieved at a current density of $\approx 55 \text{ mA/cm}^2$ using the column filled with 198 g of biochar and an anolyte volume of 1.45 L. Much higher current densities can be obtained using the proposed technique as the anodic process of ferrous iron oxidation is decoupled from the carbon oxidation process. Nine electrolysis-regeneration cycles were successfully performed to prove the proposed concept. The CO_2 production rate achieved in this study was up to 98% of the stoichiometric value proposed for the iron-mediated carbon-assisted water electrolysis.

More than 5000 organic compounds were produced in the process; however, only carboxylic acids were identified in this study. Further investigations are required to identify all types of products formed in biochar-assisted water electrolysis.

It is also important to identify and investigate other possible methods of carbon reactivation (e.g., chemical or mechanochemical) with low energy consumption or/and to optimize the thermal reactivation to reduce its energy demand.

4. EXPERIMENTAL SECTION

4.1. Reagents. FeCl_3 , FeCl_2 , H_2SO_4 (98%), HCl (37%), NaOH , and other analytical reagents were used as received from Merck and Sigma-Aldrich. Commercial apple-tree biochar was ground, sieved to obtain particles of 2–4 mm size, washed using the deionized water, and dried overnight at 60 °C. The chemical composition of charcoal used in this study is shown in Table 5.

4.2. Batch-Mode Experiments of Fe(III) Reduction by Charcoal. Reduction of ferrous iron by apple-tree biochar was studied first using batch-mode experiments. The purpose of this part of the study was to obtain the composition of the anolyte solution optimal for the process shown in Figure 2. The batch-mode experiments were performed in 250 mL stoppered glass bottles in a temperature-regulated shaking water bath (MRC BT-350) to keep the temperature constant at 25 ± 0.1 °C (shaking rate of 125 rpm). The volume of the ferric iron solution in each test was 100 mL, and the biochar loading was 150 g/L. The Fe(III) reduction was studied at an initial ferric chloride concentration of 20 g Fe/kg H_2O at varied HCl and H_2SO_4 concentrations (5, 2.5, 1, 0.1 M HCl ; 0.01 and 1.0 M H_2SO_4). Samples of electrolyte solutions were withdrawn periodically during each test and analyzed for the concentration of ferrous iron.

4.3. Experimental System for Biochar-Assisted Iron-Mediated Water Electrolysis. The electrochemical system schematically shown in Figure 2 was constructed and operated in this study. The catholyte solution (1 L) comprised hydrochloric acid (1 M) and sodium chloride (63.2 g/L). The anolyte solution (1.45 L) comprised hydrochloric acid (1 M) and ferric chloride at an initial concentration of 20 g Fe/kg H_2O . The temperature of the anolyte solution was controlled using a heating mantle controlled by the thermocouple installed in a glass pocket of the anolyte holding vessel. During the operation, the electrolyte solution was recirculated between the holding vessels, the biochar column (anolyte

only), and the electrolysis cell using a two-channel peristaltic pump (36 mL/min, Masterflex 6–600 rpm, 16" L/S Norprene tubing). Figure 8 shows the photo image of the laboratory setup.

To determine the amount of CO_2 gas produced during the electrolysis process, the headspace of the anolyte holding vessel was continuously flushed with pure nitrogen gas (N_2 99.999%, Maxima) that was subsequently bubbled into the 0.2 M NaOH solution (1.25 L) using the sintered glass gas diffuser. In addition, the peristaltic pump recirculated the NaOH solution between the holding vessel and a condenser column installed on top of the NaOH vessel to enhance the gas absorption efficiency. To ensure complete CO_2 absorption, the gas outlet of the first CO_2 -absorption unit was bubbled through the 0.2 M NaOH solution (0.5 L) in another vessel (not shown in Figure 8) connected in series to the first unit.

The current efficiency for hydrogen gas production was studied in a separate set of short experiments conducted using the large biochar column at constant current (12.5, 25, 37.5, and 50 mA/cm^2) operations. The volume of the electrochemically produced H_2 gas was measured using the water displacement method. The current efficiency for the hydrogen evolution reaction (CE_{H_2} , %) was calculated from a duration of the electrolysis process (t , s), current (I , A), and the volume of generated H_2 gas (V_{H_2} , L) using Faraday's law of electrolysis (eq 17) assuming an ideal gas behavior of the $\text{H}_2(\text{g})$

$$\text{CE}_{\text{H}_2} = \frac{V_{\text{H}_2}(\text{L})}{22.4 \left(\frac{\text{L}}{\text{mol H}_2} \right)} \cdot 2 \left(\frac{\text{mol e}^-}{\text{mol H}_2} \right) \cdot 96485 \left(\frac{\text{C}}{\text{mol e}^-} \right) \cdot \frac{1}{I(\text{A}) \cdot t(\text{s})} \times 100 \quad (17)$$

A custom-made divided flow-through electrochemical cell was applied in the system shown in Figures 2 and 8. The active area of parallel rectangular electrodes was 20 cm^2 , and they were separated by a Nafion 117 proton exchange membrane. The current collector of the anodic side was a platinum-coated titanium plate (thickness: 3 mm, area 90 cm^2) with an engraved flow channel (depth 2 mm, width 3 mm, and 36 cm overall length). The anode located on top of the Pt/Ti plate was a titanium felt (Bekaert, fiber diameter 22 μm , thickness 0.9 mm, porosity 77%, area 20 cm^2) coated with a platinum catalyst. The current collector of the cathodic side was an epoxy-impregnated graphite plate (thickness: 10 mm, area 90 cm^2) with an engraved flow channel (depth 2 mm, width 3 mm, and 36 cm overall length). The cathode was a carbon paper (Teflon-treated Toray TGP-60, thickness 0.15 mm, and area 20 cm^2) loaded with a platinum black catalyst (catalyst loading: 0.6 mg/cm^2). Graphite felt (AvCarb Material Solutions, thickness 3.2 mm, area 20 cm^2) was inserted between the graphite current collector and the electrode to ensure low contact resistance.

Two Pyrex glass-made biochar columns were used in this study. The larger column had an external diameter of 38.1 mm and a length of 53 cm. The external diameter and length of the smaller column were 22.1 mm and 25 cm, respectively. To prevent an escape of charcoal particles from columns, their both sides were closed by adapters equipped with porous sintered glass discs (pore size 100–160 μm).

Every experiment conducted in the system shown in Figure 8 had one or two stages. Within a single-stage operation, the

anolyte solution was recirculated through the biochar column with no current flowing in the electrolysis cell. At the second stage, the electrolyzer was operated at a constant voltage of 1.0 V (provided by Metrohm Autolab, PGSTAT302N). At this cell potential, no detrimental chlorine evolution reaction⁴³ can occur at the anode because its reversible potential at 80 °C is 1.28 V.

The two-stage operation comprised both operational stages performed sequentially. Samples of electrolyte solutions were withdrawn periodically in every experiment using an autosampler and analyzed for ferrous iron concentration. The NaOH solutions were periodically sampled as well and analyzed for inorganic carbon concentration.

4.4. Preparation of Deactivated Biochar. To prepare deactivated biochar, the larger column was filled with 198 g of as-received biochar, and the two-stage operation was performed until complete depletion of the biochar ability to reduce ferric iron (as was indicated by very low electrolysis current density of <5 mA/cm²). Next, the biochar in the large column was washed with hydrochloric acid (1 M), acidified water (HCl, pH = 2.0), and deionized water to remove all iron species from the biochar. Afterward, the biochar was dried, removed from the column, and stored dry until further tests.

4.5. Thermal Reactivation of Biochar. Thermal reactivation of deactivated charcoal in a nitrogen atmosphere was studied at 250, 350, and 450 °C. In every test, 30 g of deactivated charcoal was placed into the metal tube (stainless-steel 316, internal diameter 53 mm, length 18.5 cm) that was purged with nitrogen gas to remove all oxygen prior to each experiment. The gauge pressure of the nitrogen gas inside the tube was maintained constant at 2 bar during the regeneration of the biochar in the furnace (Thermo Scientific, Thermolyne Furnace F600). In each test, the heating step, which lasted for 1.5 h, was followed by the 6 h long treatment at the desired temperature. During an additional experiment conducted at 450 °C for 7.5 h (including 1.5 h of preheating), the effluent gas was bubbled through the NaOH adsorption unit and the solution was periodically sampled and analyzed for the concentration of inorganic carbon.

4.6. Evaluation of Biochar Reactivation Efficiency. To compare the efficiency of biochar reactivation obtained at different temperatures, the small column was packed with a portion of the reactivated biochar (≈22 g) and an anolyte solution (70 °C, HCl 1.0 M, 20 g Fe/kg H₂O of ferric chloride, 1.5 L) was recirculated through it until the concentration of ferrous iron reached the steady state.

4.7. Cycling CAWE-Regeneration Operations. Once the optimal reactivation temperature (450 °C, see Section 2) was obtained in reactivation experiments, the overall process shown in Figure 2 (excluding the preparation of biochar and its application to soil) was studied in repeated electrolysis-regeneration operations using the same portion of the biochar in all cycles. In these experiments, the small column filled with 21.83 g of biochar reactivated at 450 °C was operated at 70 °C in a two-stage operation mode. First, the anolyte (HCl 1.0 M, 20 g Fe/kg H₂O of ferric chloride) was recirculated through the column (no electric current was applied in the electrolysis cell within this stage). Next, the electrolysis stage was performed for at least 15 h at a constant cell potential of 1.0 (V). Afterward, the biochar column was sent to the regeneration step. Prior to the regeneration, the anolyte was drained from the column, but no washing of the biochar was applied. Afterward, the column with biochar was heat-treated

using the horizontal high-temperature oven (Carbolite Gero Ltd.). The biochar was first dried in the nitrogen flux (10 mL/min) at 95 °C for 12 h. Next, the regeneration was performed at 450 °C (heating to 450 °C—1.5 h, treatment at 450 °C—3 h). The nitrogen gas exiting the biochar column during the reactivation step was passed through the CO₂-absorption system to determine the CO₂ production rates. After the regeneration, the column was cooled to room temperature, weighted to assess the biochar loss, and reinstalled into the electrochemical system, and the experiment was repeated. Overall, nine electrolysis-reativation cycles were performed.

4.8. Analytical Methods. The concentration of ferrous ions was determined using the modified phenanthroline method.⁴⁴ Total organic carbon (TOC) and inorganic carbon (IC), were measured using a Sievers M5310 C TOC Analyzer with detection ranges of 0.04–50 mg/L for TOC and 0.04–100 mg/L for IC. Ash content was analyzed according to the standard method.⁴⁵ Elemental analysis was performed using the Flash 2000 Organic elemental analyzer (Thermo Scientific). An attempt was made to analyze organic compounds that were accumulated during the electrolysis-regeneration cycles in NaOH solutions. For this task, the solution was analyzed by a VARIAN CP-3800 GC instrument with an FID detector, autosampler CP-8400, and a Thermo (TG-WAXMS A) column (length 30 m, I.D. 0.25mm, film 0.25 μm).

X-ray photoelectron spectroscopy (XPS) analyses were performed in UHV (2.5 × 10⁻¹⁰ Torr base pressure) using 5600 Multi-Technique System (PHI). The sample was irradiated with an Al Kα monochromatic source (1486.6 eV), and the outcome electrons were analyzed by a spherical capacitor analyzer using the slit aperture of 0.8 mm. The samples were analyzed at the surface only. They were charged during the measurements, and this charging was compensated by a charge neutralizer (additional mathematical shifting was used to reference the C 1s peak to 285 eV energy of hydrocarbons).

AUTHOR INFORMATION

Corresponding Author

Youri Gendel – Faculty of Civil and Environmental Engineering, The Technion Israel Institute of Technology, Haifa 32000, Israel; orcid.org/0000-0002-1332-6646; Email: ygendel@tx.technion.ac.il

Authors

Gidon Amikam – Faculty of Civil and Environmental Engineering, The Technion Israel Institute of Technology, Haifa 32000, Israel

Noga Fridman-Bishop – Faculty of Civil and Environmental Engineering, The Technion Israel Institute of Technology, Haifa 32000, Israel

Complete contact information is available at: <https://pubs.acs.org/10.1021/acsomega.0c04820>

Notes

The authors declare no competing financial interest.

ACKNOWLEDGMENTS

This research received no specific grant from any funding agency in the public, commercial, or not-for-profit sectors.

REFERENCES

- (1) Ju, H. K.; Badwal, S.; Giddey, S. A comprehensive review of carbon and hydrocarbon assisted water electrolysis for hydrogen production. *Appl. Energy* **2018**, *231*, 502–533.
- (2) IEA Hydrogen. Hydrogen Production & Distribution. 2007. <https://webstore.iea.org/iea-energy-technology-essentials-hydrogen-production-distribution>.
- (3) Krishna, R. H. Review of Research on Production Methods of Hydrogen: Future Fuel. *Eur. J. Biotechnol. Biosci.* **2013**, *1*, 84–93.
- (4) Carmo, M.; Fritz, D. L.; Mergel, J.; Stolten, D. A comprehensive review on PEM water electrolysis. *Int. J. Hydrogen Energy* **2013**, *38*, 4901–4934.
- (5) Çelik, D.; Meltem, Y. Investigation of hydrogen production methods in accordance with green chemistry principles. *Int. J. Hydrogen Energy* **2017**, *42*, 23395–23401.
- (6) IEA Hydrogen. Special Reports: Global Trends and Outlook for Hydrogen. 2017. <http://ieahydrogen.org/PUBLICATIONS,-REPORTS-PRESENTATIONS/Special-Reports.aspx>.
- (7) Buttler, A.; Spliethoff, H. Current status of water electrolysis for energy storage, grid balancing and sector coupling via power-to-gas and power-to-liquids: A review. *Renewable Sustainable Energy Rev.* **2018**, *82*, 2440–2454.
- (8) Millet, P. Fundamentals of Water Electrolysis. In *Hydrogen Production: Electrolysis*; Wiley-VCH Verlag GmbH & Co. KGaA, 2015; Vol. 2, pp 33–62.
- (9) O'Brien, J. A.; Hinkley, J. T.; Donne, S. W.; Lindquist, S. E. The electrochemical oxidation of aqueous sulfur dioxide: A critical review of work with respect to the hybrid sulfur cycle. *Electrochim. Acta* **2010**, *55*, 573–591.
- (10) Gorenssek, M. B.; Staser, J. A.; Stanford, T. G.; Weidner, J. W. A thermodynamic analysis of the SO₂/H₂SO₄ system in SO₂-depolarized electrolysis. *Int. J. Hydrogen Energy* **2009**, *34*, 6089–6095.
- (11) Kamal, M. H.; Khundkar, M. Electrolysis oxidation of peat. *Fuel* **1966**, *45*, 9.
- (12) Park, S. Electrochemistry of Carbonaceous Materials and Coal (Review). *J. Electrochem. Soc.* **1984**, *131*, 363C–373C.
- (13) Farooque, M.; Coughlin, R. W. Electrochemical gasification of coal. *Fuel* **1979**, *58*, 705–712.
- (14) Coughlin, R. W.; Farooque, M. Hydrogen production from coal, water and electrons. *Nature* **1979**, *279*, 301–303.
- (15) Coughlin, R. W.; Farooque, M. Electrochemical Gasification of Coal—Simultaneous Production of Hydrogen and Carbon Dioxide by a Single Reaction Involving Coal, Water, and Electrons. *Ind. Eng. Chem. Process Des. Dev.* **1980**, *19*, 211–219.
- (16) Coughlin, R. W.; Farooque, M. Thermodynamic, kinetic, and mass balance aspects of coal-depolarized water electrolysis. *Ind. Eng. Chem. Process Des. Dev.* **1982**, *21*, 559–564.
- (17) Seehra, M. S.; Ranganathan, S.; Manivannan, A. Carbon-assisted water electrolysis: an energy-efficient process to produce pure H₂ at room temperature. *Appl. Phys. Lett.* **2007**, *90*, No. 044104.
- (18) Baldwin, R. P.; Jones, K. F.; Joseph, J. T.; Wong, J. L. Voltammetry and electrolysis of coal slurries and H-coal liquids. *Fuel* **1981**, *60*, 739–743.
- (19) Okada, G.; et al. On the Electrolysis of Coal Slurries. *J. Electrochem. Soc.* **1981**, *128*, 2097–2102.
- (20) Dhooge, P. M.; et al. Electrochemical Studies of Coal Slurry Oxidation Mechanisms. *J. Electrochem. Soc.* **1982**, *129*, 1719–1724.
- (21) Atkins, P. W.; de Paula, J.; Keeler, J. *Atkins' Physical Chemistry*, 9th ed.; Oxford University Press, 2018.
- (22) Hesenov, A.; Meryemoglu, B.; Içten, O. Electrolysis of coal slurries to produce hydrogen gas: Effects of different factors on hydrogen yield. *Int. J. Hydrogen Energy* **2011**, *36*, 12249–12258.
- (23) Yu, P.; Botte, G. G. Bimetallic platinum-iron electrocatalyst supported on carbon fibers for coal electrolysis. *J. Power Sources* **2015**, *274*, 165–169.
- (24) Wang, C.; Zhao, Y.; Zhou, W.; Liu, H.; Yin, R. Electro-oxidation of coal on NiO and/or Co₃O₄ modified TiO₂/Pt electrodes. *Electrochim. Acta* **2011**, *56*, 6299–6304.
- (25) Jin, X.; Botte, G. G. Understanding the kinetics of coal electrolysis at intermediate temperatures. *J. Power Sources* **2010**, *195*, 4935–4942.
- (26) Yu, T.; Lu, S.; Zhou, W.; Cao, W.; Fan, C. Q.; Yin, R. Catalytic effect of K₃Fe(CN)₆ on hydrogen production from coal electro-oxidation. *Electrochim. Acta* **2012**, *83*, 485–489.
- (27) Patel, C. R. P.; Tripathi, P.; Vishwakarma, A. K.; Talat, M.; Soni, P. K.; Yadav, T. P.; Srivastava, O. N. Enhanced hydrogen generation by water electrolysis employing carbon nano-structure composites. *Int. J. Hydrogen Energy* **2018**, *43*, 3180–3189.
- (28) Hesenov, A.; Kinik, H.; Puli, G.; Gozmen, B.; Irmak, S.; Erbatur, O. Electrolysis of coal slurries to produce hydrogen gas: Relationship between CO₂ and H₂ formation. *Int. J. Hydrogen Energy* **2011**, *36*, 5361–5368.
- (29) Seehra, M. S.; Bollineni, S. Nanocarbon boosts energy-efficient hydrogen production in carbon-assisted water electrolysis. *Int. J. Hydrogen Energy* **2009**, *34*, 6078–6084.
- (30) Seehra, M. S.; Akkineni, L. P.; Yalamanchi, M.; Singh, V.; Poston, J. Structural characteristics of nanoparticles produced by hydrothermal pretreatment of cellulose and their applications for electrochemical hydrogen generation. *Int. J. Hydrogen Energy* **2012**, *37*, 9514–9523.
- (31) Ge, L.; Gong, X.; Wang, Z.; Zhao, L.; Wang, Y.; Wang, M. Insight of anode reaction for CWS (coal water slurry) electrolysis for hydrogen production. *Energy* **2016**, *96*, 372–382.
- (32) Ju, H.; Giddey, S.; Badwal, S. P. Role of iron species as mediator in a PEM based carbon-water co-electrolysis for cost-effective hydrogen production. *Int. J. Hydrogen Energy* **2018**, *43*, 9144–9152.
- (33) Figueiredo, J. L. Functionalization of porous carbons for catalytic applications. *J. Mater. Chem. A* **2013**, *1*, 9351–9364.
- (34) Carabineiro, S. A. C.; Fernando, M.; Pereira, R.; Órfão, J. J. M.; Figueiredo, J. L. Surface Chemistry of Activated Carbons. *Chem. Phys. Res. J.* **2011**, *4*, 1935–2492.
- (35) Fan, X.; Lu, Y.; Xu, H.; Kong, X.; Wang, J. Reversible redox reaction on the oxygen-containing functional groups of an electrochemically modified graphite electrode for the pseudo-capacitance. *J. Mater. Chem.* **2011**, *21*, 18753–18760.
- (36) Fowles, M. Black carbon sequestration as an alternative to bioenergy. *Biomass Bioenergy* **2007**, *31*, 426–432.
- (37) Matovic, D. Biochar as a viable carbon sequestration option: Global and Canadian perspective. *Energy* **2011**, *36*, 2011–2016.
- (38) Gurwick, N. P.; Moore, L. A.; Kelly, C.; Elias, P. A. Systematic Review of Biochar Research, with a Focus on Its Stability in situ and Its Promise as a Climate Mitigation Strategy. *PLoS One* **2013**, *8*, No. e75932.
- (39) Pröll, T.; Al Afif, R.; Schaffer, S.; Pfeifer, C. Reduced Local Emissions and Long-term Carbon Storage through Pyrolysis of Agricultural Waste and Application of Pyrolysis Char for Soil Improvement. *Energy Procedia* **2017**, *114*, 6057–6066.
- (40) Chen, L.; Nakamoto, R.; Kudo, S.; Asano, S.; Hayashi, J.-i. Biochar-assisted water electrolysis. *Energy Fuels* **2019**, *33*, 11246–11252.
- (41) Stoddard, W. B., Jr. Iron Plating. *Trans. Electrochem. Soc.* **1943**, *84*, 305–318.
- (42) Díaz, S. L.; Calderon, J. A.; Barcia, O. E.; Mattos, O. R. Electrodeposition of iron in sulphate solutions. *Electrochim. Acta* **2008**, *53*, 7426–7435.
- (43) Amikam, G.; Nativ, P.; Gendel, Y. Chlorine-free alkaline seawater electrolysis for hydrogen production. *Int. J. Hydrogen Energy* **2018**, *43*, 6504–6514.
- (44) Herrera, L.; Ruiz, P.; Aguillon, J. C.; Fehrmann, A. A new spectrophotometric method for the determination of ferrous iron in the presence of ferric iron. *J. Chem. Technol. Biotechnol.* **1989**, *44*, 171–181.
- (45) American Society for Testing and Materials. *Standard Test Method for Ash in the Analysis Sample of Coal and Coke from Coal* (ASTM D 3174 Reapproved); ASTM International: West Conshohocken, PA, 1996.